Proceedings of the ASME 2022 International Technical Conference and Exhibition on Packaging and Integration of Electronic and Photonic Microsystems
InterPACK2022
October 24-28, 2022, Anaheim, California

IPACK2022-97172

DRAFT

COMPARATIVE ANALYSIS OF DIRECT AND INDIRECT COOLING OF WIDE-BANDGAP POWER MODULES AND PERFORMANCE ENHANCEMENT OF JET IMPINGEMENT–BASED DIRECT SUBSTRATE COOLING

Himel Barua
Building and Transportation Science Division

Oak Ridge National Laboratory, Oak Ridge, Tennessee, USA

Emre Gurpinar
Building and Transportation Science Division

Oak Ridge National Laboratory, Oak Ridge, Tennessee, USA

Lingxiao Xue
Building and Transportation Science Division

Oak Ridge National Laboratory, Oak Ridge, Tennessee, USA

Burak Ozpineci
Building and Transportation Science Division

Oak Ridge National Laboratory, Oak Ridge, Tennessee, USA

ABSTRACT

With the development of high-power and high-torque machines, requirements for high–power density electronics are increasing. Thermal management of such systems requires high heat extraction. Conventional air cooling based heat sinks and cold plate based liquid cooling have their own benefits for various applications but has limitations for high power density applications. The current study explores a jet impingement based direct substrate cooling system that was implemented for a SiC based direct bonded Cu substrate for various power losses. Numerical comparison between jet impingement cooling and conventional horizontal/indirect cooling (pin fin heat sink and genetic algorithm–optimized heat sink) showed that the area weighted average of the heat transfer coefficient (HTC) is high for both horizontal cooling designs, and the local HTC is higher for jet impingement. Design iterations were undertaken to resolve the bottleneck of this cooling system. Increasing the number of nozzles helped to cover more area at the direct bonded Cu bottom plate, which drops the chip temperature considerably. With a constant flow rate, increasing the number of nozzles would decrease local jet velocity, which reduces the heat extraction by jet impingement. This issue can be addressed by reducing the diameter of nozzle but doing so results in a high pressure drop where the design constraint is 2 psi. A diverging nozzle design is proposed, which has a higher spreading angle of the jet that increases the flow coverage and reduces the pressure drop of the coolant loop.

Keywords: Wide-bandgap device, direct substrate cooling, jet impingement

NOMENCLATURE

ρ	Density
T	Temperature
k	Thermal conductivity
u	Velocity
μ	Viscosity
σ	Stress
c_p	Specific heat
Q	Heat source

1. INTRODUCTION

Transportation electrification requires improvements in system efficiency and power density. To achieve high-power density, it is required to have advanced power conversion modules that use the most efficient semiconductor devices along with optimal thermal management systems. With the rapid market adoption of electric vehicles, the US Department of Energy targets include more than eight times increase in the power density of traction inverters [1]. To achieve this challenging goal, wide bandgap (WBG) devices have been extensively researched to improve the power density of the power modules [2], [3] and advanced thermal management concepts are proposed to minimize the heatsink size [4].

Although WBG devices operate at 96%–99% efficiency, they are not completely loss-free, and the loss eventually dissipate as heat. However, increments of power output and reduction in the size of electric components will add additional thermal management challenges that result in decreased reliability, decreased efficiency and potential failure. Decreased reliability and efficiency would cause higher conduction loss at higher temperatures since the resistance between source and drain is a function of temperature.

To address these thermal reliability issues, numerous solutions are available and widely used in power electronics applications, including heat sink, cold plates, air cooling, and liquid jets [5]. Generally, power electronics modules are cooled by horizontal cooling channels or cold plates [6]; the flow path can be linear, serpentine style, moving back and forth, or have different shapes [7], [8], [9]. Adding complexity in the flow paths like making the flow path serpentine or allowing to cover more space increases the flow coverage which reduces the junction temperature in expense of adding higher pressure drop. With increasing operating switching frequency for WBG devices and the expectation to dissipate 1,000 W/cm^2 [10] with current devices reaching 500 W/cm^2 [11], [12], cooling systems are required to address high heat flux. Horizontal cooling technologies generally produce heat transfer coefficients (HTCs) around 20,000 W/m^2-K but with higher volume size due to the size of heat sink, channels or cold plate whereas vertical cooling technologies such as jet impingement can reach 115,000 W/m^2-K or even higher [13] with smaller liquid volume.

Table 1. Comparison between horizontal and vertical cooling

Cooling methods	HTC (Average) (kW/m^2-K)	Pressure drop	Volume
Horizontal	~20	Lower	Higher
Vertical	~20-200	High	Lower

Table 1 shows comparison between horizontal and vertical cooling method. Figure 1 shows the arrangement of cooling systems for conventional power modules. In indirect cooling systems (Fig. 1(a) and (b)), the coolant is not directly attached to the module; rather, it is exposed to a heat sink, which is attached with a module through a thermal interface material (TIM). TIMs generally have low thermal conductivity, and the conductivity varies according to the pressure [14]. Jet impingement cooling can be used for direct cooling techniques to remove the heat sink and corresponding TIM layer. Removing these two layers reduces the thermal resistance significantly (~30% [5]) since the heat sink interface and TIM layer are the largest contributors of thermal resistance in the power module stack. Although jet impingement is widely used for cooling applications such as gas turbines [15] and braking systems [16], it is not widely used for power electronics [17], mainly because of its higher pressure drop [18]. Numerous studies have been conducted on jet impingement cooling for applications such as solar energy [19], [20], electric motors [21], [22], and electronics chips [17], [23], [24]. For jet impingement cooling, different design and operating parameters such as the jet diameter [25], [26], nozzle to plate spacing [22], [27], spacing between jets [24], number of jets [11] and cross-sectional area of jets [28], [29], have influential effects. Increasing jet diameter with same flow rate would reduce the heat extraction rate and lower the pressure drop. Increasing spacing between jet nozzle outlet and impact surface would decrease heat extraction. Increasing number of jets and decreasing the spacing between them would increase heat extraction but the flow rate has to be modified accordingly. Some studies have compared the effect of a single jet to multiple jets [24], free surface to submerged jets [22], [23], and water jets to dielectric and polymer jets and sprays. Dielectric and polymer jets can be impacted directly into the chip surface which can directly cool the device.

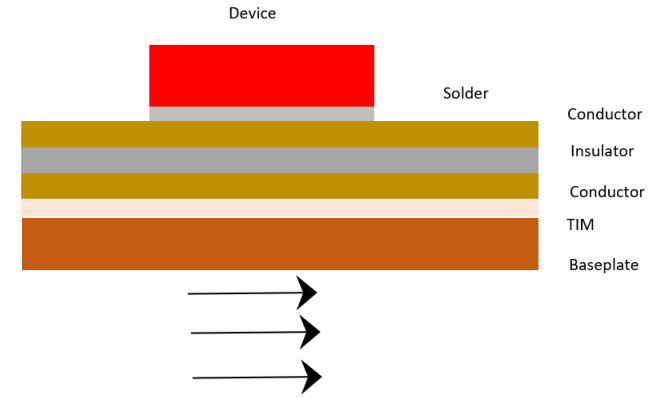

(a)

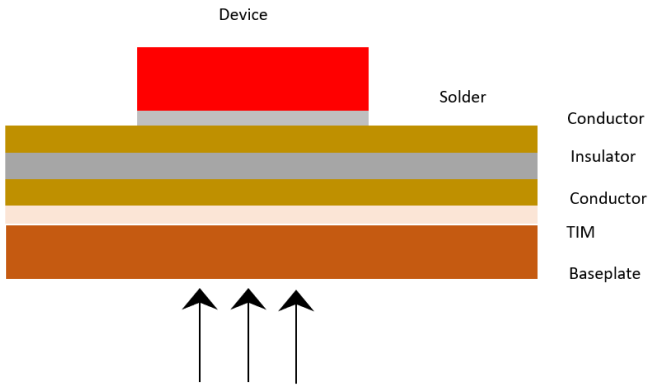

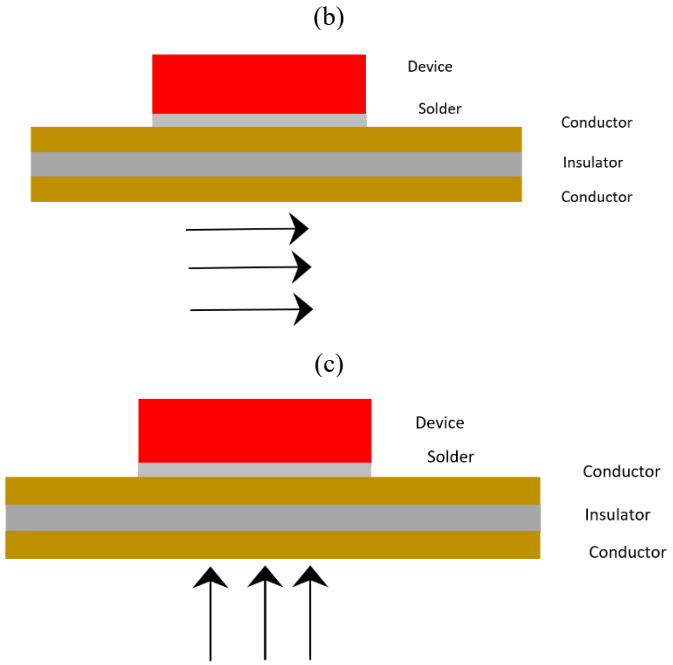

Fig. 1. (a) Horizontal indirect, (b) vertical indirect, (c) Horizontal direct and (d) vertical direct substrate cooling.

In this study, jet impingement was implemented for direct substrate cooling to a WBG device embedded on a direct bonded Cu (DBC) structure. As mentioned, jet impingement cooling is a well-established method but has shortcomings in power electronics applications. This article addresses two of the major drawbacks of this process—small heat transfer area and pressure drop—and describes the methodical design iteration to resolve these issues. Section 2.1 describes the physical structure of the jet and the implementation process in direct substrate cooling of the power module and section 2.2 describes model development Section 3.1 describes the primary results for conventional jet impingement for the full-scale model. Section 3.2 describes the design modifications undertaken to enhance thermal performance. Section 3.3 provides a comparison between horizontal indirect cooling and vertical direct substrate cooling. Finally, Section 4 provides conclusions and plans for future work.

2. THEORY AND MODELING

2.1 Jet characteristics

In jet impingement cooling, high-velocity coolant ejects from a nozzle or an orifice plate [30] perpendicular to the impingement surface. The impingement surface can be in certain angle for oblique jets [31]. The impact of the liquid stream yields a highly concentrated heat removal rate at the impact zone, which cools a small area that dissipates high heat flux. When the jet impacts the target surface, two different flow points/regions develop near the impact surface: the stagnation point (i.e., impingement point) and the wall jet region (Fig. 2). At the stagnation point, the impinging flow changes its trajectory and becomes radially accelerating flow owing to the pressure gradient. This change causes higher heat transfer because of boundary layer thinning. At the wall jet zone, the radial flow decelerates, and the heat transfer rate decreases along the flow direction. One of the drawbacks of jet impingement cooling is the difference of heat transfer rate between the stagnation point and wall jet region. In this study, this drawback was considered, and an array of jets were deployed to reduce the nonuniformity of heat flux.

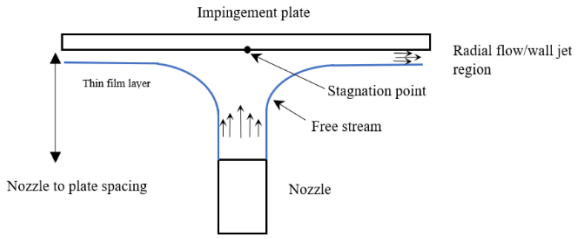

Fig. 2. Jet structure and different zones of jet flow

The primary geometric and design parameters that can characterize jet flow are the jet hole diameter, channel/nozzle height, channel/nozzle width, jet hole pitch (the distance between two consecutive nozzles), and number of jets.

Figure 3(a) shows the full-scale model of power module device with the cooling system and Figure 3(b) shows the side view and the chip footprint. The model (see Fig. 3(a) and (b)) includes a power module with two SiC devices. Each device has a total power loss of 100 W, which corresponds to a heat flux of 316 W/cm^2. Both devices are placed at the top of the DBC substrate. The DBC layer contains a Cu layer at the top, an AlN layer, and a Cu layer at the bottom. Devices are soldered with the top Cu layer. The fluid domain is placed just below the bottom layer. Table 1 shows the design parameters for the DBC substrate. A 50:50 ethylene glycol: water mixture was used as coolant.

Table 2. Design parameters

Component	**Thickness (mm)**	**Area (mm^2)**
SiC	0.18	31.65
Top Cu layer	0.45	1,227.48
Middle AlN layer	0.64	3,963.9
Bottom Cu layer	0.45	1,754.2
Solder	0.05	31.65

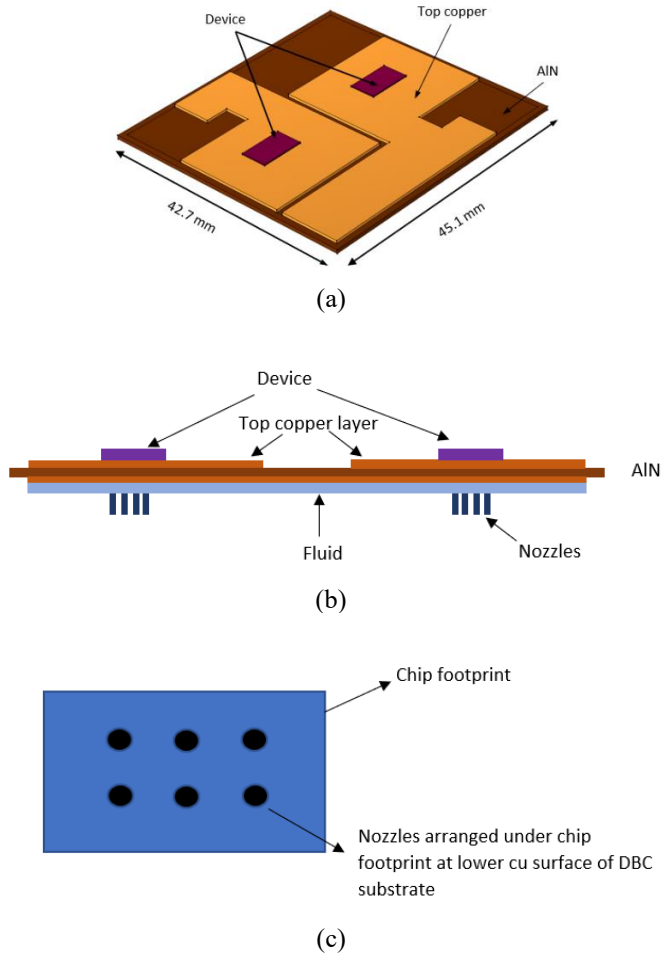

Fig. 3. (a) Full-scale model of power module device; (b) side view of (top) the DBC stack and (c) nozzles at (bottom) the chip footprint (six nozzles).

2.2 Model development

The scope of this work is limited to numerical study. To resolve the fluid flow and heat transfer conservation of mass, momentum and energy equations were solved. Heat conduction equation was solved to determine the heat flow through the solid domain. Fluid flow and heat transfer equations were coupled. One of the constraints in the design was to keep the flow regime as a laminar flow, where the corresponding jet Reynolds number is less than 2,300. All the design and flow parameters were selected for the corresponding Reynolds number for the jet to be less than 2,300.

$$Re = \frac{\rho v d}{\mu} \tag{1}$$

where Re is the Reynolds number, ρ is the density of the jet liquid, v is the velocity of the jet, d is the diameter of the nozzle, and μ is the viscosity of the liquid. All the parameters are considered as functions of temperature, except density. The flow was considered incompressible because the corresponding Mach number is less than 0.3. To resolve the fluid flow and heat transfer following equations has been solved. A Finite element software, COMSOL has been used as solver.

Conservation of mass:

$$\frac{\partial \rho}{\partial t} + \nabla \cdot (\rho u) = 0 \tag{2}$$

Conservation of momentum:

$$\frac{\partial (\rho u)}{\partial t} + \nabla \cdot (\rho u\, u) = \nabla \cdot \sigma + \rho f \tag{3}$$

Conservation of energy:

$$\rho C_p \frac{(\partial T)}{\partial t} + \rho C_p u \cdot \nabla T = \nabla \cdot (k \nabla T) + Q \tag{4}$$

Local heat transfer coefficient, h(x,y) has been calculated by

$$h(x,y) = \frac{Q(x,y)}{A(T(x,y) - T_{ambient})} \tag{5}$$

To calculate the global/average heat transfer coefficient, area averaged surface heat transfer coefficient is calculated by the following equation

$$h = \left[\frac{1}{A}\int\int\left(\frac{1}{h(x,y)}dxdy\right)\right]^{-1} \tag{6}$$

Here, A is the surface area at the bottom DBC surface (bottom copper wall where jet impacts), h is the global heat transfer coefficient.

3. DESIGN EVOLUTION RESULTS AND DISCUSSION

A numerical study was conducted to understand the effects of different design and operating parameters of a jet impingement cooling system. A basic flow system was designed with two manifolds (inlet and outlet) and 12 circular channels in between them (6 circular channel for each chip). To reduce computational time, the lower manifold (Inlet manifold) was discarded from the final model. The inlet velocity of each nozzle was calculated by using a conservation of mass considering the flow as incompressible and uniform. The initial model had 12 nozzles; for each chip, 6 nozzles were used (Fig. 3(b) bottom). For the coolant flow rate of 1.6 L/min, the maximum chip temperature was 106°C.

Figure 4(b) shows the HTC and temperature at the bottom substrate Cu layer where the jet impinged directly. The maximum HTC recovered from the surface was 195 kW/m^2-K. The high-HTC zone was very small and was only the circular impact zone. The 3D HTC plot (Fig. 5(b)) shows high-HTC peak

zones in the bottom Cu surface. On the same surface, negative/reverse peaks of the temperature zone were observed.

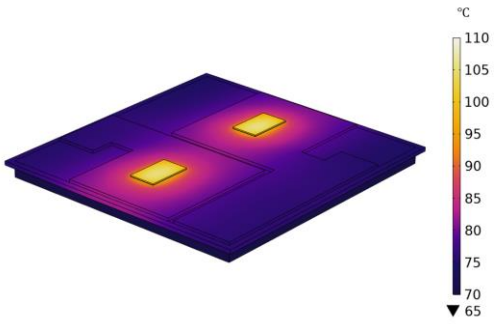

(a)

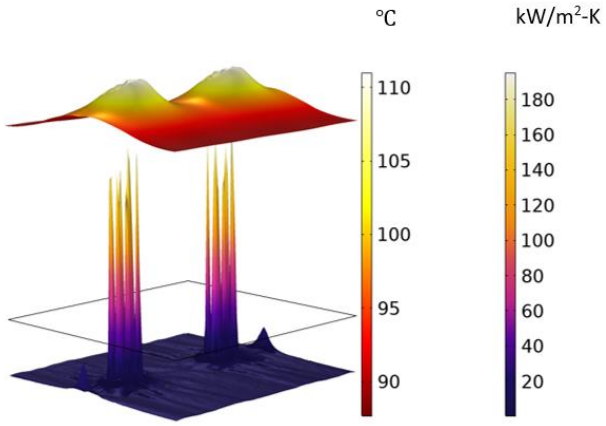

(b)

Fig. 4. (a) Temperature distribution on the domain; (b) HTC and temperature distribution at the bottom layer of the DBC substrate.

Figure 5(a) shows the temperature distribution at the top and bottom of the device surface, bottom of the DBC substrate (at bottom Cu layer). At the top and bottom of the chip surface, the temperature was parabolic (high at the middle of the chip and lower near the edge) and the temperature difference was 1°C across the chip thickness (180 μm). At the chip footprint in the bottom of the DBC substrate, the temperature profile is more sinusoidal, where at each of the impingement points, there is a steeper temperature drop than in the surrounding area.

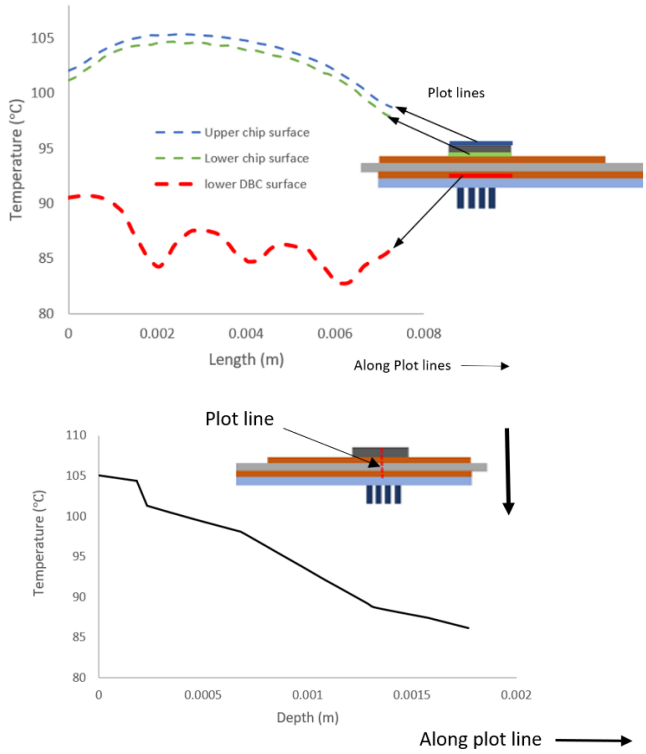

Fig. 5. (a) Temperature distribution at the top and bottom surface of the device, and at the bottom of the DBC substrate (interface of jet and substrate); (b) temperature drop along the depth of the substrate (from top chip surface to bottom DBC surface).

Figure 6 shows that at each negative/reverse temperature (red dotted line) peak, there is a corresponding HTC (blue solid line) peak. At each HTC peak, because of high heat extraction, there is a corresponding temperature valley. This oscillation of temperature can cause thermal imbalance, but the magnitude difference is within 3°C. Figure 6 shows promising values of the local HTC, which was considerably large compared with the HTC values available in the literature for single-phase liquid cooling. However, the challenge of this cooling system is its very small heat transfer area, which was at the stagnation point of the jet in this case. The global average HTC at the bottom DBC surface was 6.34 kW/m^2-K, whereas at the impingement surface, the local HTC was 200 kW/m^2-K—approximately 33 times higher than the average HTC.

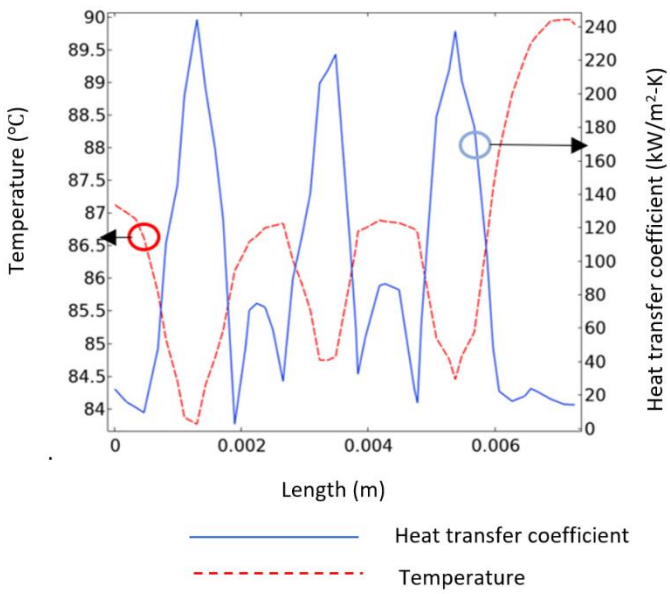

Fig. 6. Temperature and HTC distribution at the bottom DBC layer.

Besides thermal performance, another influential design parameter in electronics cooling systems is pressure drop. Pressure drop is affected by several design and operating parameters, including diameter of the nozzle, flow rate, coolant properties, nozzle design, and temperature. Figure 7 shows pressure drop and velocity variation along the centerline, parallel to the flow direction of the nozzle.

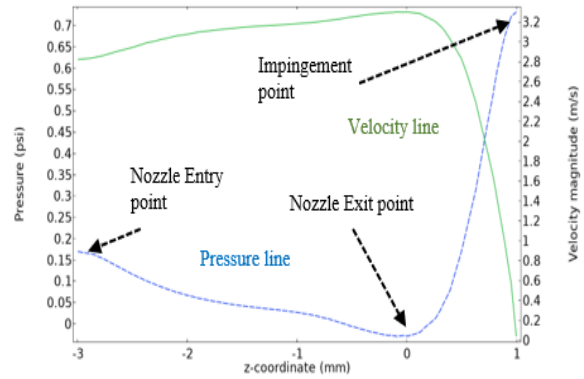

(a)

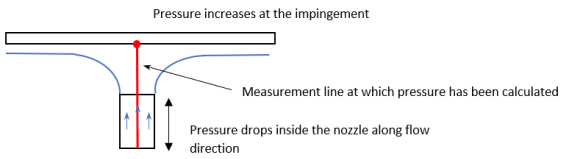

(b)

Fig. 7. (a) Pressure drop and velocity distribution along the centerline of the nozzle for 3.2 L/min flow rate and (b) plot line along the centerline of nozzle

In Fig. 7, the dashed blue line represents pressure drop, and the solid green line represents velocity. The measurement line was taken from the nozzle inlet up to the stagnation point. The gradient of pressure from nozzle inlet to outlet shows a linear decrease, but from nozzle outlet to stagnation point, there was an exponential increase owing to conversion of kinetic energy to pressure. The corresponding velocity line shows the velocity at the middle of the nozzle. The velocity increased along the nozzle length because of the gradual formation of the boundary layer and the transition toward fully developed flow. However, at the exit of the nozzle, because of the sudden expansion of flow (jet coming out from the nozzle to open space), velocity dropped exponentially, and at the stagnation point, it was zero. Although the total pressure drop from system inlet to outlet was 0.25 psi, the local pressure profile shows that at the stagnation point, the pressure drop can be nearly 3 times larger than the global average pressure drop, which could lead to an error in pressure drop calculation for such a system. For 3.2 L/min flow rate, the global pressure drop was 0.25 psi, whereas for 1.6 L/min flow rate, it was ~0.10 psi, which is far lower than the threshold of 2 psi.

3.1 Model size reduction

To quantify thermal performance, one of the key performance criteria is HTC. Because HTC varies with time and space, for a steady-state case, the average HTC was considered. For a highly localized system like jet impingement, accurately quantifying the average HTC and comparing it with other cooling systems is difficult. Jet impingement nozzles were placed only in the chip footprint, which is the hot spot in the power module package. The average HTC was calculated by taking the average of the whole bottom DBC surface (where the coolant impinged) (see Eqn. 6), which decreased the HTC value because of the low jet coverage. To reduce this penalization, a reduced model was developed in which the computational domain is 2.5 times larger in terms of volume than the original model. Figure 8 (a) shows the heat spreading through DBC structure and 8(b) and (c) shows the different views of the reduced model used for future modeling.

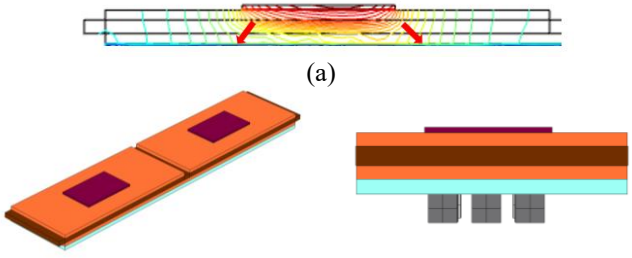

(a)

(b) (c)

Fig. 8 (a) Heat spreading in angular fashion (45°); (b) isometric view and (c) side view of the reduced substrate model with chips.

The reduced model consisted of both heat sources and chips. Only the sides of the DBC substrate were reduced to consider the

surfaces near the chip, the high heat transfer area which most effectively transfers heat.

3.2 Performance improvement and design evolution

The initial evaluation of the jet impingement cooling system and the relative comparison with a horizontal cooling system demonstrate that although a high magnitude of local HTC could be achieved via jet impingement, this phenomenon was very localized, and overall performance was not satisfactory because of the low fluid coverage, which is one of the major strengths of the horizontal liquid cooling system. The pressure drop was also considerably higher than in other horizontal flow cooling systems. However, with improved and more clinical designs, these issues can be resolved. Numerous design iterations were conducted to improve the performance; design parameters included the number of nozzles, shape of the nozzle along the flow direction, and nozzle diameter.

Figure 10 shows the design evolution and corresponding temperature evolution of the device. Figure 10(a) shows the temperature distribution for the reduced size model. Because of the reduction of area (70% surface area), heat dissipation decreased, and corresponding chip temperature increased. The maximum temperature was 152°C for the reduced model and 127°C for the full model for a flow rate of 1.6 L/min and a jet velocity of 2.82 m/s. To improve the flow coverage from the first reduced order model with 6 nozzles per chip, in the next design iteration, the number of nozzles per chip was doubled (12 nozzles per chip). With the same flow rate and doubled number of nozzles, the nozzle exit velocity for each nozzle was reduced to 1.41 m/s, and the junction temperature lowered to 135°C (17°C lower than the initial configuration). As discussed in Section 2.1, for jet flow, the heat transfer at impingement points was directly influenced by the impinged flow velocity. Because increasing the number of nozzles reduced the jet velocity for a constant flow rate, to leverage the increased number of nozzles, the flow rate was doubled (3.2 L/min). For the 3.2 L/min flow rate in the configuration with 12 nozzles per chip and a jet velocity of 2.81 m/s, the junction temperature lowered to 118°C, which is 34°C lower than the initial configuration. For the 1.6 L/min flow rate in the configuration with 12 nozzles per chip and a jet velocity of 2.81 m/s, the corresponding pressure drop was 0.5 psi. For the 3.2 L/min flow rate, the pressure drop increased to ~1.7 psi. Although both pressure drops are less than 2 psi, with the higher flow rate, the pressure drop was closer to the threshold value. Pressure drop in this system was not influenced by the number of nozzles as long as the flow rate was constant.

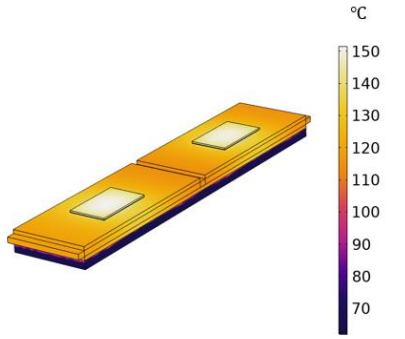

(a) Reduced model with 6 nozzles per chip

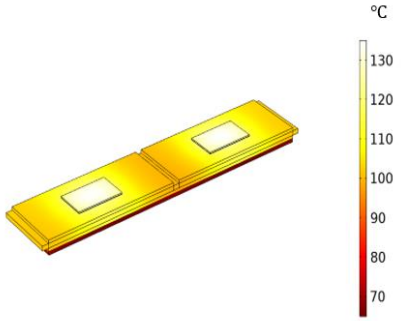

(b) Reduced model with 12 nozzles per chip at a flow rate of 1.6 L/min

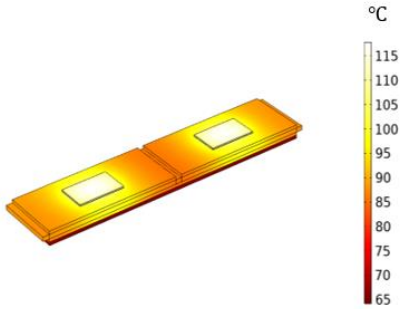

(c) Reduced model with 12 nozzles per chip at a flow rate of 3.2 L/min

Fig. 10. Effect of nozzle number and flow rate on junction temperature.

Increasing the number of nozzles would cover more area and would increase the heat transfer rate from the interface, as well as the corresponding chip temperature. However, this change increases the pressure drop owing to an increase in flow rate to keep the jet velocity constant. An approach to overcome this challenge would be to modify the spreading pattern of the coolant so that it can spread more and cover more area while keeping the pressure drop within the threshold. Diverging nozzles were considered in which the exit diameter was larger than the inlet diameter of the nozzle, which creates a diverging shape.

Figure 11 shows the location, orientation, and design of the diverging nozzles. The exit cross-sectional area of the nozzle was larger than the inlet cross-sectional area. The relationship

between inlet and outlet area can be described by area ratio. Here, two area ratios were studied: 1:2 and 1:3. The 1:3 area ratio nozzle design showed the best performance in terms of junction temperature for a 3.2 L/min flow rate; the junction temperature reduced to 90°C, but the corresponding pressure drop was very high, so the design was not used. In terms of thermal and pressure drops, the best design was for the 1:2 area ratio with a 3.2 L/min flow rate.

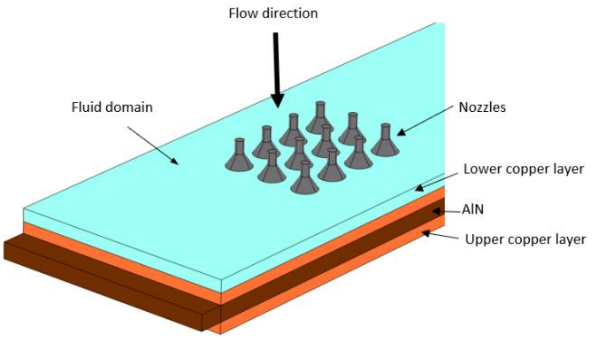

(a)

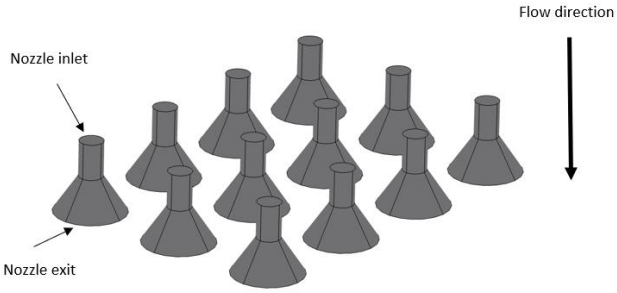

(b)

Fig. 11. Diverging nozzles at the bottom of the DBC substrate, and (b) diverging nozzle design (zoomed out view).

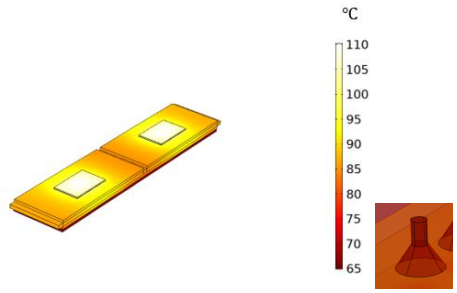

(a)

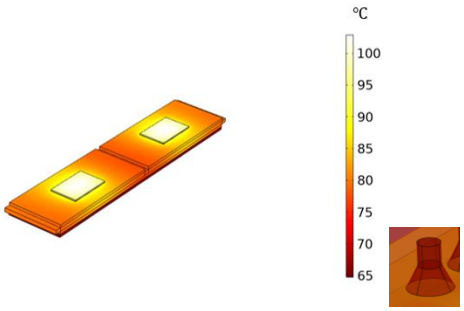

(b)

Fig. 12. (a) Flow rate of 1.6 L/min with area ratio of 1:3, and (b) flow rate of 3.2 L/min with area ratio of 1:2.

Figure 12 shows the temperature distribution for nozzle design with area ratio 1:3 for flow rate 1.6 L/min which has higher junction temperature than the nozzle design with area ratio 1:2 for flow rate 3.2 L/min. Figure 13 shows pressure drop along the flow rate until 0.5 mm length, where the flow exits the nozzle and at 1 mm impinges on the bottom DBC surface. At the stagnation point, pressure was 1.5 psi for the 1.6 L/min flow rate, and 6 psi for the 3.2 L/min flow rate. The overall pressure drop in the system for the area ratio of 1:2 and flow rate of 3.2 L/min was 0.96 psi.

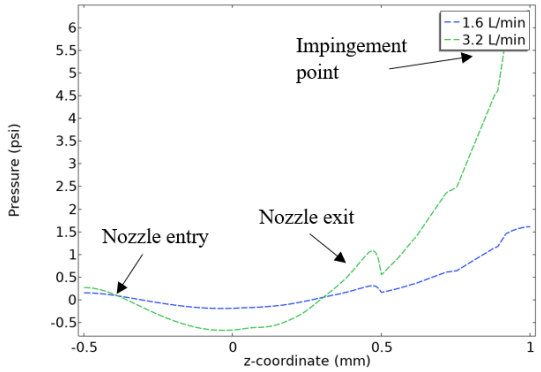

Fig. 13. Pressure drop along the centerline of the nozzle along the flow direction for 1:2 area ratio nozzles.

Because the scope of this work is limited to simulation, a mesh independent study was undertaken for the reduced jet impingement model for three mesh sizes. The accuracy evaluation matrix contained the junction temperature and the

flow pressure drop from jet inlet to system outlet. For the three mesh iterations, the error margin was within ~5%.

3.3 Comparison of results between jet impingement cooling and horizontal cooling

To evaluate the performance of the jet impingement cooling system, a comparison was made with two other cases in which the cooling system was horizontal and the heat sink was attached with the bottom DBC layer by TIM. In case 1, the jet impingement cooling system was compared with a pin fin heat sink cooling system; in case 2, it was compared with a GA-optimized liquid cooling heat sink [4]. In the pin fin heat sink, 55 pins were used, and the total height of the heat sink was 12 mm (baseplate 4 mm and pin fin 8 mm). For the GA-optimized heat sink, the maximum heat sink height was 15 mm. The flow rate was 1.6 L/min for both cases. The volume of the GA-optimized heat sink was 1.7 times smaller than that of the pin fin heat sink. For the sake of comparison, the evolved design for the jet impingement case was used, which had 12 diverging nozzles with the 1:2 area ratio and a flow rate of 3.2 L/min. Fig. 14 shows the comparison between the jet impingement cooling and pin fin heat sink and GA optimized heat sink cooling. With modified design jet impingement shows lower junction temperature than other two design.

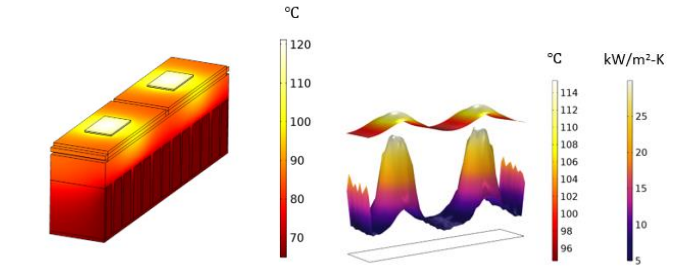

(a)

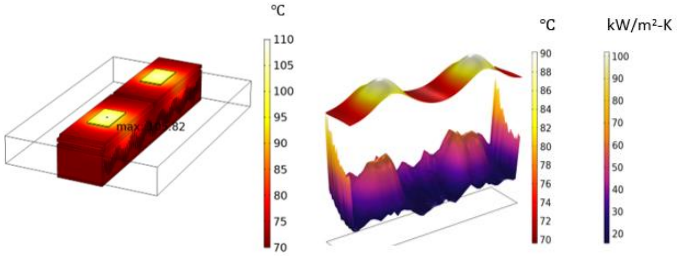

(b)

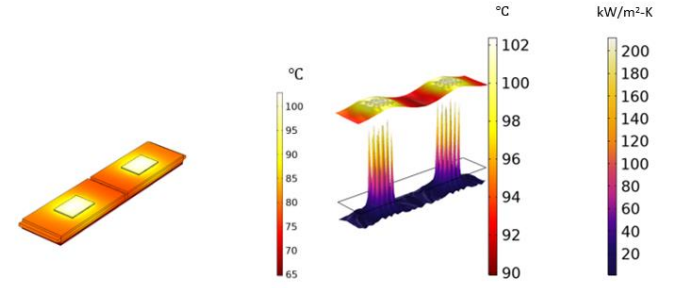

(c)

Fig. 14. Comparison of temperature distribution and temperature, HTC distribution at lower DBC surface for the (a) pin fin heat sink horizontal cooling system, (b) GA-optimized heat sink horizontal cooling system, and (c) jet impingement cooling system (12 diverging nozzles per chip, 3.2 L/min flow rate).

Table 3 Comparison of junction temperature and local maximum heat transfer coefficient for different designs

Design	Flow rate (L/min)	Junction temperature (°C)	Local HTC at impingement surface (kW/m^2-K)
Pin fin heat sink	1.6	120	30
GA optimized heat sink	1.6	110	100
Full scale model	1.6	110	180
6 nozzles/chip	1.6	156	190
12 nozzles/chip	1.6	130	200
12 nozzles/chip	3.2	115	202
12 nozzles/chip Area ratio: 1:2	3.2	100	210
12 nozzles/chip Area ratio: 1:3	1.6	110	220

Table 3 summarizes the comparison between horizontal indirect cooling for pin fin, GA optimized heat sink and direct substrate cooling by jet impingement for different nozzle number and flow rates.

4. CONCLUSION AND FUTURE WORK

This article presents a comprehensive study on implementing a vertical cooling system for direct substrate cooling. Jet impingement was used for vertical cooling. In direct substrate cooling, coolant was impinged directly in the lower DBC surface which removes the heat sink and TIM layer. This reduces the thermal resistance ~ 30% comparing with indirect cooling. Direct substrate cooling results indicate that although jet impingement shows a high heat transfer rate, because of the low flow coverage, it is not very suitable for high–power density WBG devices. Furthermore, the pressure drop was higher than conventional horizontal flow cooling. By increasing the number of nozzles per chip and increasing flow rate to keep the jet velocity constant, the junction temperature reduced considerably. Using diverging nozzles instead of straight nozzles increased the flow coverage at the chip footprint, which further reduced the junction temperature and pressure drop. The jet impingement system was compared with two horizontal cooling systems with different heat sinks: a conventional pin fin heat sink and a GA-optimized liquid heat sink. The comparison showed

that the configuration with 12 diverging nozzles (area ratio of 1:2) per chip and a 3.2 L/min flow rate performed better than both horizontal cooling designs. The power density for the jet impingement cooling system was also 2 times higher than in the pin fin heat sink cooling system and 0.8 times higher than in the GA-optimized heat sink cooling system. Future work will include implementing an optimization algorithm to determine the optimized distribution of different nozzle diameters and shapes to improve thermal performance.

ACKNOWLEDGEMENTS

This material is based upon work supported by the US Department of Energy's (DOE's) Vehicle Technologies Office Electric Drive Technologies Program. The authors thank Ms. Susan Rogers of DOE for her support and guidance.

REFERENCES

[1] Electrical and Electronics Technical *Team Roadmap*. (2017). www.uscar.org.
[2] L. L. Xue, G. J. Su, and B. Ozpineci, "DC-Ripple-energy adaptive-minimization (DREAM) modulation scheme for a high-power density inverter," *Conference Proceedings - IEEE Applied Power Electronics Conference and Exposition - APEC*, pp. 186–191, Jun. 2021, doi: 10.1109/APEC42165.2021.9487324.
[3] S. Chowdhury, E. Gurpinar, and B. Ozpineci, "Capacitor Technologies: Characterization, Selection, and Packaging for Next-Generation Power Electronics Applications," IEEE Transactions on Transportation Electrification, Jun. 2022, doi: 10.1109/TTE.2021.3139806.
[4] R. Sahu, E. Gurpinar, and B. Ozpineci, "Liquid-Cooled Heat Sink Optimization for Thermal Imbalance Mitigation in Wide-Bandgap Power Modules," *Journal of Electronic Packaging*, vol. 144, no. 2, Jun. 2022, doi: 10.1115/1.4052068.
[5] C. Qian et al., "Thermal Management on IGBT Power Electronic Devices and Modules," *IEEE Access*, vol. 6, pp. 12868–12884, 2018, doi: 10.1109/ACCESS.2018.2793300.
[6] J. Broughton, V. Smet, R. R. Tummala, and Y. K. Joshi, "Review of Thermal Packaging Technologies for Automotive Power Electronics for Traction Purposes," *Journal of Electronic Packaging, Transactions of the ASME*, vol. 140, no. 4, 2018, doi: 10.1115/1.4040828/366154.
[7] Y. P. Zhang, X. L. Yu, Q. K. Feng, and R. T. Zhang, "Thermal performance study of integrated cold plate with power module," *Applied Thermal Engineering*, vol. 29, no. 17–18, 3568–3573, 2009, doi: 10.1016/J.APPLTHERMALENG.2009.06.013.
[8] A. Fouad and M. Al-Neama, "Serpentine Minichannel Liquid-Cooled Heat Sinks for Electronics Cooling Applications," PhD thesis, University of Leeds, 2018.
[9] X. Hao, B. Peng, G. Xie, and Y. Chen, "Thermal analysis and experimental validation of laminar heat transfer and pressure drop in serpentine channel heat sinks for electronic cooling," *Journal of Electronic Packaging, Transactions of the ASME*, vol. 136, no. 3, 2014, doi: 10.1115/1.4027508.
[10] I. Mudawar, "Assessment of high-heat-flux thermal management schemes," *IEEE Transactions on Components and Packaging Technologies*, vol. 24, no. 2, pp. 122–141, 2001, doi: 10.1109/6144.926375.
[11] "GS66508T Top-side cooled 650 V E-mode GaN transistor Datasheet," GaN Systems, 2004. Available: https://gansystems.com/wp-content/uploads/2020/04/GS66508T-DS-Rev-200402.pdf.
[12] S. Jones-Jackson, R. Rodriguez, and A. Emadi, "Jet Impingement Cooling in Power Electronics for Electrified Automotive Transportation: Current Status and Future Trends," *IEEE Transactions on Power Electronics*, vol. 36, no. 9, pp. 10420–10435, 2021, doi: 10.1109/TPEL.2021.3059558.
[13] A. J. Robinson, "A thermal-hydraulic comparison of liquid, microchannel and impinging liquid jet array heat sinks for high-power electronics cooling," *IEEE Transactions on Components and Packaging Technologies*, vol. 32, no. 2, pp. 347–357, 2009, doi: 10.1109/TCAPT.2008.2010408.
[14] "Thermal resistance of interface materials as a function of pressure," Electronics Cooling. Available: https://www.electronics-cooling.com/1996/09/thermal-resistance-of-interface-materials-as-a-function-of-pressure/ (accessed Apr. 18, 2022).
[15] M. Forster and B. Weigand, "Experimental and numerical investigation of jet impingement cooling onto a concave leading edge of a generic gas turbine blade," *International Journal of Thermal Sciences*, vol. 164, p. 106862, 2021, doi: 10.1016/J.IJTHERMALSCI.2021.106862.
[16] O. F. P. Lyons, D. B. Murray, and A. A. Torrance, "Air jet cooling of brake discs," *Proceedings of the Institution of Mechanical Engineers, Part C: Journal of Mechanical Engineering Science*, vol. 222, no. 6, pp. 995–1004, 2008, doi: 10.1243/09544062JMES927.
[17] S. V. J. Narumanchi, V. Hassani, and D. Bharathan, "Modeling Single-Phase and Boiling Liquid Jet Impingement Cooling in Power Electronics," 2005, Accessed: May 09, 2022. [Online]. Available: http://www.osti.gov/bridge
[18] A. Blinov, D. Vinnikov, T. Lehtla, A. Blinov, D. Vinnikov, and T. Lehtla, "Cooling Methods for High-Power Electronic Systems," *SJRUP*, vol. 29, no. 1, pp. 79–86, 2011, doi: 10.2478/V10144-011-0014-X.
[19] A. Royne and C. J. Dey, "Effect of nozzle geometry on pressure drop and heat transfer in submerged jet arrays," *International Journal of Heat and Mass Transfer*, vol. 49, no. 3–4, pp. 800–804, 2006, doi: 10.1016/J.IJHEATMASSTRANSFER.2005.11.014.
[20] H. M. S. Bahaidarah, "Experimental performance evaluation and modeling of jet impingement cooling for thermal management of photovoltaics," *Solar Energy*, vol. 135, pp. 605–617, 2016, doi: 10.1016/J.SOLENER.2016.06.015.
[21] B. Kekelia, "Jet Impingement Cooling of Electric Machines with Driveline Fluids," 2021. Available:

https://www.allianceforsustainableenergy.org/about.html (accessed Apr. 19, 2022)
[22] "Jet impingement cooling of electric motor end-windings." Patent US20030102728A1. Available: https://patents.google.com/patent/US20030102728 (accessed Apr. 19, 2022).
[23] "Dielectric jet impingement cooling of electronic chips," *Proceedings of the 34th ASME National Heat Transfer Conference*, 2000.
[24] B. Kwon, T. Foulkes, T. Yang, N. Miljkovic, and W. P. King, "Air Jet Impingement Cooling of Electronic Devices Using Additively Manufactured Nozzles," *IEEE Transactions on Components, Packaging and Manufacturing Technology*, vol. 10, no. 2, pp. 220–229, 2020, doi: 10.1109/TCPMT.2019.2936852.
[25] D. J. Womac, S. Ramadhyani, and F. P. Incropera, "Correlating Equations for Impingement Cooling of Small Heat Sources With Single Circular Liquid Jets," *Journal of Heat Transfer*, vol. 115, no. 1, pp. 106–115, 1993, doi: 10.1115/1.2910635.
[26] D. J. Womac, S. Ramadhyani, and F. P. Incropera, "Correlating Equations for Impingement Cooling of Small Heat Sources with Single Circular Liquid Jets," *Journal of Heat Transfer*, vol. 115, no. 1, pp. 106–115, 1993, doi: 10.1115/1.2910635.
[27] N. R. Saad, S. Polat, and W. J. M. Douglas, "Confined multiple impinging slot jets without crossflow effects," *International Journal of Heat and Fluid Flow*, vol. 13, no. 1, pp. 2–14, 1992, doi: 10.1016/0142-727X(92)90054-D.
[28] D. W. Colucci and R. Viskanta, "Effect of nozzle geometry on local convective heat transfer to a confined impinging air jet," *Experimental Thermal and Fluid Science*, vol. 13, no. 1, pp. 71–80, 1996, doi: 10.1016/0894-1777(96)00015-5.
[29] D. Singh, B. Premachandran, and S. Kohli, "Effect of nozzle shape on jet impingement heat transfer from a circular cylinder," *International Journal of Thermal Sciences*, vol. 96, pp. 45–69, 2015, doi: 10.1016/J.IJTHERMALSCI.2015.04.011.
[30] M. S. Shin, S. Senguttuvan, and S. M. Kim, "Investigations of Flow and Heat Transfer Characteristics in a Channel Impingement Cooling Configuration with a Single Row of Water Jets," *Energies*, vol. 14, no. 14, art. no. 4327, 2021, doi: 10.3390/EN14144327.
[31] A. Mishra, H. Yadav, L. Djenidi, and A. Agrawal, "Experimental study of flow characteristics of an oblique impinging jet," *Experiments in Fluids*, vol. 61, no. 3, pp. 1–16, 2020, doi: 10.1007/S00348-020-2923-Y/FIGURES/16.